Biophysical Journal, Volume *119*

Supplemental Information

Cryo-EM and Molecular Docking Shows Myosin Loop 4 Contacts Actin and Tropomyosin on Thin Filaments

Matthew H. Doran, Elumalai Pavadai, Michael J. Rynkiewicz, Jonathan Walklate, Esther Bullitt, Jeffrey R. Moore, Michael Regnier, Michael A. Geeves, and William Lehman

Species/myosin isoform	Residues																								
Sarcomeric myosins 2	**359**	**360**	**361**	**362**	**363**	**364**	**365**	**366**	**367**	**368**	**369**	**370**	**371**	**372**	**373**	**374**		**375**	**376**	**377**	**378**	**379**	**380**	**381**	**382**
Bovine MyHC-β – slow skeletal, cardiac	F	G	N	M	K	F	K	L	K	Q	R	E	E	Q	A	E	-	P	D	G	T	E	E	A	D
Human MyHC-β – slow skeletal, cardiac	F	G	N	M	K	F	K	Q	K	Q	R	E	E	Q	A	E	-	P	D	G	T	E	E	A	D
Human MyHC-2x fast skeletal	Y	G	N	M	K	F	K	Q	K	Q	R	E	E	Q	A	E	-	P	D	G	T	E	V	A	D
Human MyHC-2a fast skeletal	Y	G	N	L	K	F	K	Q	K	Q	R	E	E	Q	A	E	-	P	D	G	T	E	V	A	D
Human MyHC-embryonic	Y	G	N	M	K	F	K	Q	K	Q	R	E	E	Q	A	E	-	P	D	G	T	E	V	A	D
Human MyHC-2b fast skeletal	Y	G	N	M	K	F	K	Q	K	Q	R	E	E	Q	A	E	-	P	D	G	T	E	V	A	D
Human MyHC-α fast cardiac	Y	G	N	M	K	F	K	Q	K	Q	R	E	E	Q	A	E	-	P	D	G	T	E	D	A	D
Human MyHC-perinatal	Y	G	N	M	K	F	K	Q	K	Q	R	E	E	Q	A	E	-	P	D	G	T	E	V	A	D
Human MyHC-extraocular	Y	G	N	M	K	F	K	Q	K	Q	R	E	E	Q	A	E	-	P	D	G	T	E	V	A	D
Tarantula	L	G	E	M	K	F	K	Q	R	P	R	E	E	Q	A	E	-	A	D	G	T	E	E	G	E
Drosophila melanogaster	M	G	G	M	K	F	K	Q	R	G	R	E	E	Q	A	E	-	Q	D	G	E	E	E	G	G
Caenorhabditis elegans	M	G	N	M	K	F	K	Q	R	P	R	E	E	Q	A	E	-	P	D	G	T	D	E	A	E
Scallop	M	G	E	M	K	F	K	Q	R	P	R	E	E	Q	A	E	-	S	D	G	T	A	E	A	E
Squid	L	G	E	M	K	W	K	-	-	Q	R	G	E	Q	A	E	-	A	D	G	T	A	E	A	E
Non-sarcomeric myosins 2																									
Human NM 2A	L	G	N	I	V	F	K	K	E	R	N	T	D	Q	A	S	M	P	D	N	T	A	A	Q	-
Human NM 2B	F	G	N	I	S	F	K	K	E	R	N	T	D	Q	A	S	M	P	E	N	T	V	A	Q	-
Human NM 2C	F	G	N	I	A	L	K	R	E	R	N	T	D	Q	A	T	M	P	D	N	T	A	A	Q	-
Human Smooth muscle	L	G	N	I	V	F	K	K	E	R	N	T	D	Q	A	S	M	P	D	N	T	A	A	Q	-
Saccharomyces cerevisiae	I	G	N	I	E	I	K	K	T	R	N	D	A	S	L	S	A	D	-	E	P	N	L	K	-
Schizosaccharomyces pombe	M	G	N	I	D	V	G	A	D	R	S	G	-	I	A	R	L	L	N	P	D	E	I	D	-
Dictyostelium	-	G	N	I	K	F	E	K	G	A	G	E	G	A	V	L	-	K	D	K	T	A	L	N	-

Table S1. **Multiple sequence alignment of the loop 4 region of myosin II.**

Residue numbering is based on the bovine β-myosin, MyHC-β (Q9BE39), used in this investigation The Human sarcomeric myosin 2 accession codes are: MyHC-2x – P12882.3, MyHC-2a – NP_060004.3, MyHC-embryonic – NP_002461.2, MyHC-2b – Q9Y623.2, MyHC-α – AAI32668.1, MyHC-β - NP_000248.2, MyHC-perinatal – NP_002463.2, and MyHC-extraocular – NP_003793.2. The Tarantula sequence (UniProt accession code A0A140UGH3_9ARAC) is from *Aphonopelma* used for the cryo-EM structure in Woodhead et al. (1). The *Drosophila melanogaster* sequence (UniProt accession code P05661) is based off of the embryonic isoform structure PDB 5W1A (2). The *C. elegans* sequence (UniProt accession code P12844) is from the myosin-B isoform, with a crystal structure recently obtained (3). The scallop sequence (*Argopecten irradians*) (UniProt accession code P24733) is from myosin structures PDB IDs: 2OTG, 2OS8, 1SR6, 1QVI, 1KK8, and 1S5G. The squid sequence is from the rigor state crystal structure (PDB ID; 3I5G) used to build the homology model in the main text. Human non-muscle and smooth muscle sequence UniProt accession codes are: NM 2A – P35579, NM 2B – P35580, NM 2C – Q7Z406, and smooth muscle – P35749. Sequences for *Saccharomyces cerevisiae*, UniProt P19524, *Schizosaccharomyces pombe*, Q9US16 and *Dictyostelium*, UniProt P08799, myosins are also provided. Grey highlighted residues are residues that are fully or partially conserved, while the arginine group (orange) is conserved amongst the skeletal muscle myosins and appears to shift one position earlier in the non-muscle, smooth muscle and yeast myosins. N.B. Many mammalian non-muscle thin filaments contain tropomyosin, as do yeast thin filaments; no reports identify a *Dictyostelium* tropomyosin and it lacks the highlighted arginine.

Table S2. Data collection and refinement statistics.

Cryo-EM Data Statistics	
Microscope	Titan Krios
Detector	Gatan K2 Summit Direct Detector
Voltage (kV)	300
Magnification	130,000x
Pixel Size (Å)	1.06
Defocus Range (μm)	-1.5 - -2.5
Exposure Times (s/frame)	0.2
Number of Frames (per movie)	35
Total Dose (e^-)	53
Data Processing	
Box Size (pixels)	256
Inter-box Distance (Å)	27.5
Number of Micrographs	2496
Number of Segments after Manual Picking	45,040
Segments after 2D classification	40,455
Segments after 3D classification	32,158
Symmetry Imposed	
Helical Rise (Å)	27.5
Helical Twist (^{o})	166.4
Initial Model	200 Å Featureless Cylinder

Actin-Myosin-Tropomyosin Model Validation	
Atoms	28421 (no hydrogens)
Residues	3555
Ligands	3 Mg^{2+}, 3 ADP
Bonds	
Length (Å)	0.008
Angles (^{o})	1.206
Molprobity Validation	
Molprobity score	2.42
Clash score	23.09
Rotamer Outliers (%)	0.0
Ramachandran Plot	
Outliers (%)	0.26
Allowed (%)	10.29
Favored (%)	89.45
Further Validation	
Resolution Estimation (.143 threshold) (Å)	4.2
Map Sharpening B-Factor ($Å^2$)	-105
Average B-factor ($Å^2$)	70.88

Table S3. Residues along F-actin and myosin S1 that approach each other.

Actin Residue	Residue Atom	Myosin Residue	Residue Atom	Myosin Region	Distance (Å)
TYR337	OH	VAL406	CG1	CM Loop	3.1
VAL30	CG1	VAL406	CG1	CM Loop	3.6
ALA26	CB	VAL404	CG1	CM Loop	3.6
GLU334	OE2	THR412	CB	CM Loop	4.0
TYR337	CE2	THR412	CG2	CM Loop	4.0
ASP24	OD1	LYS405	NZ	CM Loop	4.5
TYR337	OH	TYR410	CD2	CM Loop	4.7
SER350	OG	SER532	OG	Helix-Loop-Helix	3.3
LEU349	CD1	PHE540	CD1	Helix-Loop-Helix	3.5
TYR143	CD1	PRO541	CG	Helix-Loop-Helix	4.0
THR148	CG2	LYS542	CG	Helix-Loop-Helix	4.1
LEU349	CD2	MET539	CB	Helix-Loop-Helix	4.2
THR148	CB	PRO541	CG	Helix-Loop-Helix	4.2
SER350	OG	MET528	CB	Helix-Loop-Helix	4.3
SER348	OG	MET539	CE	Helix-Loop-Helix	4.5
TYR143	CE1	PHE540	CZ	Helix-Loop-Helix	4.6
THR351	CG2	MET528	SD	Helix-Loop-Helix	4.6
THR351	CG2	ILE533	CD1	Helix-Loop-Helix	4.7
MET44	CE	PRO541	CD	Helix-Loop-Helix	4.8
THR351	CG2	LYS551	NZ	Helix-Loop-Helix	4.9
SER350	OG	ILE533	CD1	Helix-Loop-Helix	5.0
THR351	CG2	ASN555	ND2	Helix-Loop-Helix	5.0
ILE330	CD1	GLU371	OE2	Loop 4	3.1
ARG147	NH2	GLU371	CD	Loop 4	3.3

Intermolecular distances are noted for the atoms in actin and myosin residues that approach each other closely (cutoff ≤ 5 Å), based on models fitted to the cryo-EM reconstruction discussed in the main text. Myosin regions located at the actin-myosin interface are named, including the Cardiomyopathy Loop (CM loop), Loop 4, and the Helix-Loop-Helix motif as displayed in Figure 1B (cf. von der Ecken et al., 2016 (4); Fujii and Namba, 2017 (5); Mentes et al., 2018 (6)).

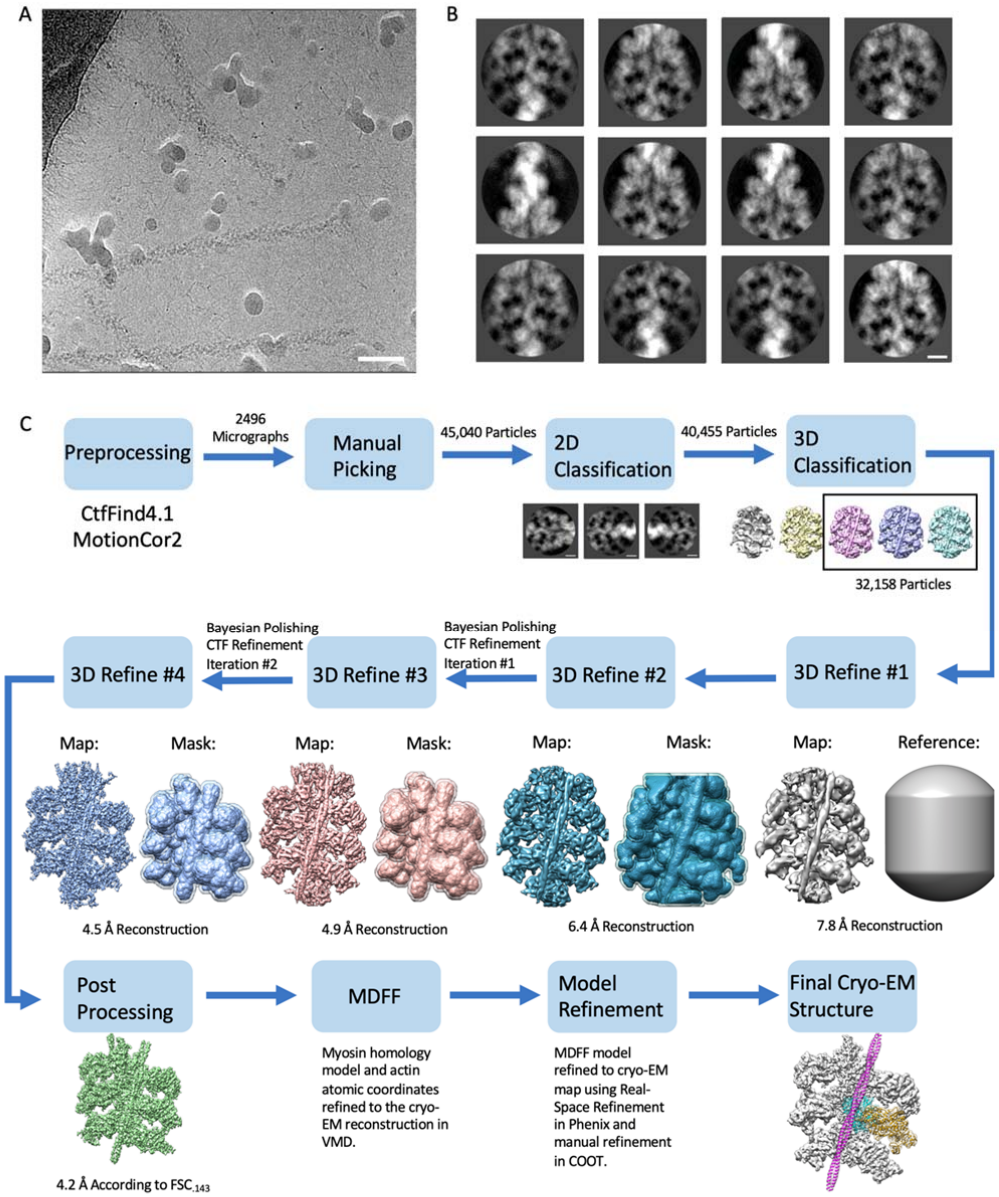

Figure S1. Cryo-EM data processing workflow.

(A) Representative micrograph of myosin S1-decorated actin-tropomyosin filaments frozen in vitreous ice. Unbound tropomyosin and myosin can be seen in the background, well separated from the filaments. Scale bar: 50 nm.

(B) Reference-free two-dimensional class averages of the actin-tropomyosin-myosin S1 segments identified in RELION 3.0.7 (7-9). The actin core of the filament along with myosin S1 arrowheads are visible. Scale bar: 5 nm.

(C) Flowchart describing the cryo-EM workflow performed in RELION 3.0.7 (7-9) that led to the 4.2 Å structure and the pseudo-atomic model of the actin-tropomyosin-myosin S1 complex. This process is also described in detail in the Materials and Methods section in the main text. Micrographs were motion corrected using MotionCor2 and the contrast transfer function (CTF) estimated and normalized by CtfFind4.1. Filaments were manually selected and divided into 270 Å long (256 pixels) overlapping segments, each offset by 27.5 Å (~90% overlap) to produce 45,040 segments. Filament segments were then sorted using two- and three-dimensional classification. Noisy or poorly defined segments were discarded. In all routines done in three-dimensions, F-actin helical symmetry was applied (166.4° subunit rotation around the F-actin helical axis and a subunit axial translation of 27.5 Å). A final set of 32,158 segments was taken for a preliminary three-dimensional refinement by first aligning these particles to a featureless 200 Å diameter cylinder, generating a 7.8 Å reconstruction. The resulting model was low-pass filtered to 60 Å to be used as a new reference for a second refinement while incorporating a solvent mask to produce a subsequent reconstruction at 6.4 Å. Two iterations of Contrast Transfer Function (CTF) refinement and Bayesian "Polishing" were then performed. Particles underwent CTF refinement with beam tilt estimation and a subset of these particles was evaluated to find optimal polishing parameters. After polishing, the optimized particles were used in the next refinement using the 6.4 Å reconstruction low-pass filtered to 60 Å as a starting model. An additional soft 6 actin-6 myosin-tropomyosin mask was employed after each iteration to focus the refinement on the central section of the acto-S1 filaments. The first iteration of CTF refinement and Bayesian polishing process re[Myosin homology model and actin atomic coordinates Refined to the cryo-EM reconstruction in VMD.] 4.9 Å resolution map. The same process was repeated once [duce a final 4.5 Å resolution map. Further iterations did not in[resolution. Final resolution estimation was made using Fourier [ation criteria, ($FSC_{0.143}$) in the RELION post processing step, wh[d a final 6-actin-6-myosin-tropomyosin map at 4.2 Å. This map was used in initial MDFF flexible fitting (10) to match a myosin homology model and F-actin model to experimental density. Refinements in PHENIX (11) and Coot (12) produced the final actomyosin

structure (see Materials and Methods section). An idealized tropomyosin coiled coil was then fitted into the density.

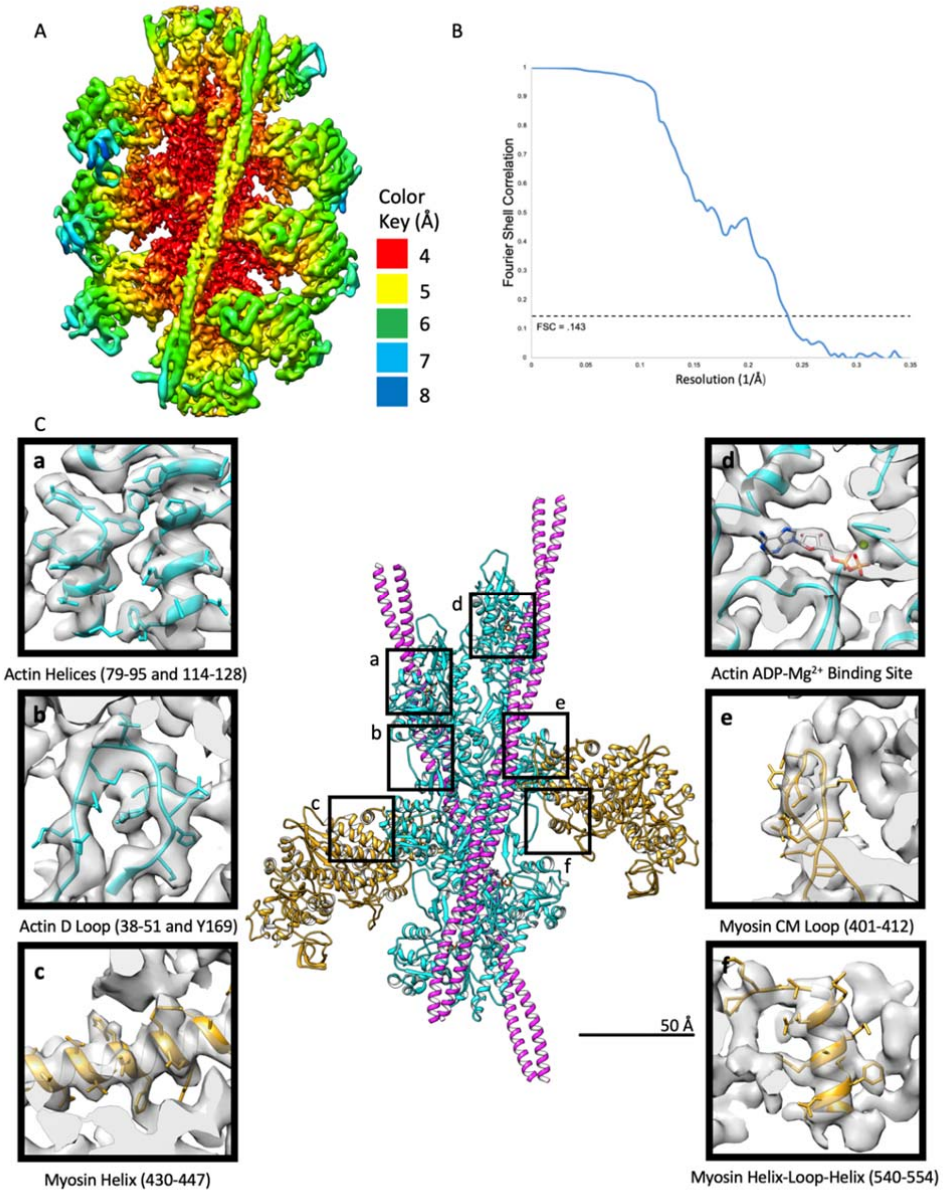

Figure S2. Local resolution of components of the reconstruction.

A. Heat map visualization showing resolution values of locally filtered data comprising the actin-tropomyosin-S1 reconstruction, calculated with the LocalRes sub-routine in RELION 3.0.7 (7-9). Actin displays the highest resolution extending to 4.0 Å, the actin-myosin interface averages a resolution of 4.5 Å, tropomyosin ranges between 5 to 6.5 Å resolution limits and the distal regions of myosin are upwards of 6 to 7 Å resolution.

B. Fourier Shell Correlation (FSC) plot of the reconstruction following final processing in RELION 3.0.7 (7-9). The calculated $FSC_{0.143}$ of 0.238 $Å^{-1}$ corresponds to a global resolution of 4.2 Å.

C. Atomic models fitted to the cryo-EM density. Selected regions of the actin-myosin complex were picked and reoriented to better display the model to map correspondence.

Figure S3. Myosin-induced sliding of tropomyosin on actin.

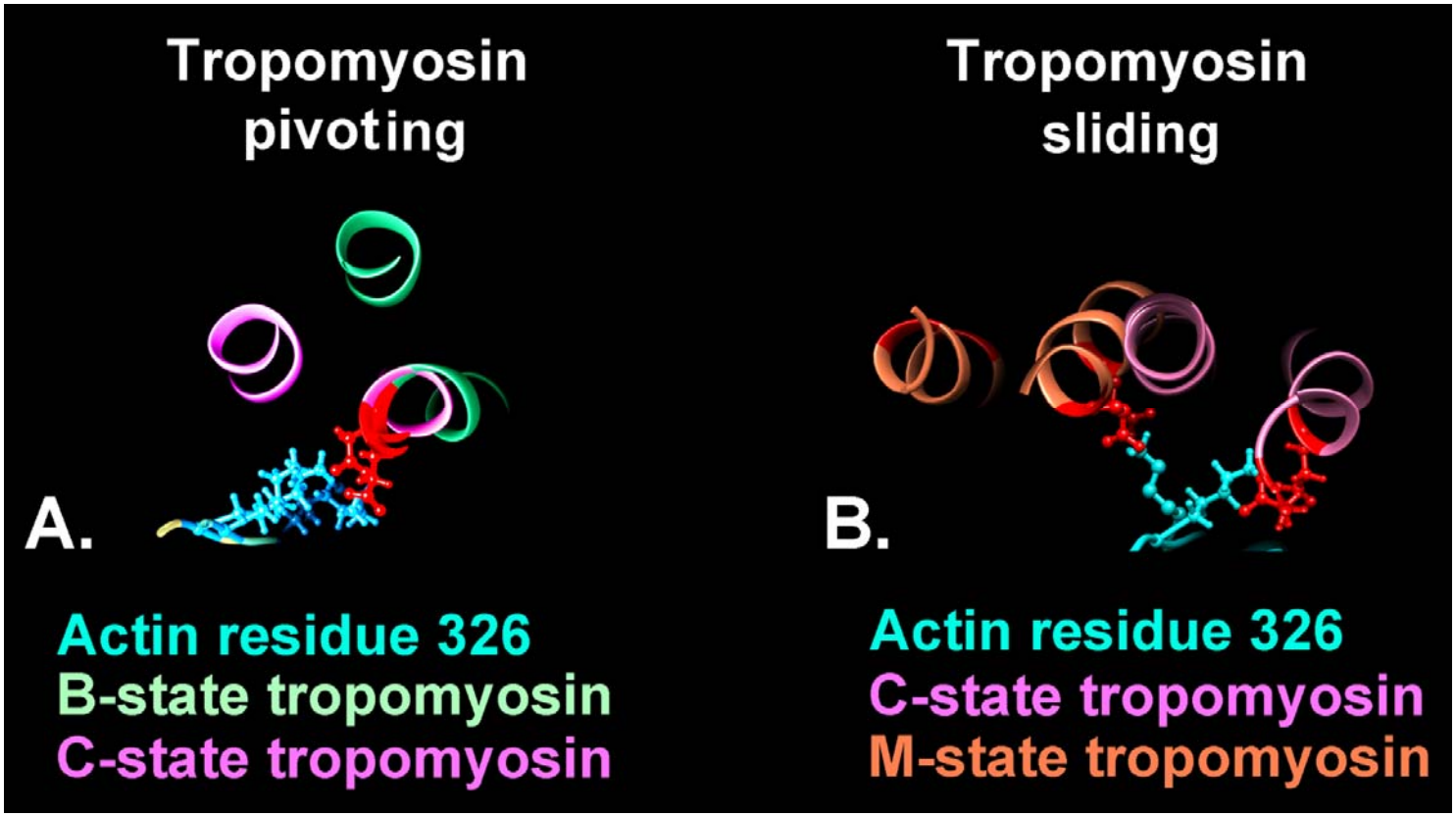

A. **B-state to C-state transition**. Superimposed transverse sections through B-state and C-state poses of the Pavadai et al. models of the thin filament (13) made at residue 326 (cyan) of actin on tropomyosin pseudo-repeat 4, showing electrostatic contacts between actin Lys326 and Glu138 of tropomyosin. Note the electrostatic contacts are between actin and the closest α-helical chain of the tropomyosin coiled coil; this chain is relatively stationary for the B/C-state transition, while the outer chains pivot between B- and C-states. Such tropomyosin pivoting characterizes the B-state/C-state transition over all pseudo-repeats except at the tropomyosin overlapping domain (13,14). Figure made from data in (13).

B. **C-state to M-state transition**. Superimposed transverse sections through C-state and M-state poses comparing the Pavadai et al. C-state model (13) and the M-state model determined in the current work, again made through residue 326 (cyan) of actin on tropomyosin pseudo-repeat 4, showing electrostatic contacts between actin Lys326 and Glu138 of C-state tropomyosin and Lys326 to Glu142 of M-state tropomyosin. Once more, electrostatic contact is made between actin and the closest of the α-helical chains of tropomyosin, but here tropomyosin pivoting is not observed and, instead, pure azimuthal sliding of the coiled coil takes place during the C/M-state transition. In fact, it is now the sidechain of Lys326 that pivots. For simplicity, the position of myosin-S1 is not shown for the M-state.

REFERENCES

1. Woodhead, J.L., F.Q. Zhao, R. Craig, E.H. Egelman, L. Alamo, and R. Padrón. 2005. Atomic model of a myosin filament in the relaxed state. *Nature.* 436:1195-1199.
2. Cadwell, J.T., D.J. Mermelstein, R.C. Walker, S.I. Berstein, and T. Huxford. 2019. X-ray crystallography and molecular dynamics analysis of Drosophia melanogaster embryonic muscle myosin define domains responsible for isoform-specific properties. *J. Mol. Biol.* 432:427-447.
3. Hellerschmied, D., A. Lehner, N. Franicevic, R. Arnese, C. Johnson, A. Vogel, A. Meinhart, R. Kurzbauer, L. Deszcz, L. Gazda, M. Geeves, and T. Clausen. 2019. Molecular features of the UNC-45 chaperone critical for binding and folding muscle myosin. *Nature Commun*. 10:4781.
4. von der Ecken J., S.M. Heissler, S. Pathan-Chhatbar, D.J Manstein, and S. Raunser. 2016. Cryo-EM structure of a human cytoplasmic actomyosin complex at near-atomic resolution. *Nature*. 534:724-728.
5. Fujii, T, and K. Namba. 2017. Structure of actomyosin rigour complex at 5.2 Å resolution and insights into the ATPase cycle mechanism. *Nat. Commun*. 2017 8:13969.
6. Mentes, A., A. Huehn, X. Liu, A. Zwolak, R. Dominguez, H. Shuman, E.M. Ostap, and C.V. Sindelar. 2018. High-resolution cryo-EM structures of actin-bound myosin states reveal the mechanism of myosin force sensing. *Proc. Natl. Acad. Sci. USA*. 115:1292-1297.
7. Scheres, S.H. 2012. RELION: implementation of a Bayesian approach to cryo-EM structure determination. *J. Struct. Biol*. 180:519-530.
8. Scheres, S.H. 2016. Processing of structurally heterogeneous Cryo-EM aata in RELION. *Methods Enzymol*. 579:125-157.
9. He, S, and S.H.W Scheres. 2017 Helical reconstruction in RELION. *J. Struct. Biol.* 198:163-176.
10. Trabuco, L.G., E. Villa, E. Schreiner, C.B. Harrison, and K. Schulten. 2009. Molecular dynamics flexible fitting: A practical guide to combine cryo-electron microscopy and x-ray crystallography. *Methods*. 49:174-180.
11. Afonine, P.V., B.K. Poon, R.J. Read, O.V.Sobolev, T.C. Terwilliger, A. Urzhumtsev, and P.D. Adams. 2018. Real-space refinement in PHENIX for cryo-EM and crystallography. *Acta Crystallogr. D Struct. Biol*. 74:531-544.
12. Emsley, P., B. Lohkamps, W.G. Scott, and K. Cowtan. 2010. Features and development of Coot. *Acta Crystall. D Struct. Biol.* 66: 486-501.
13. Pavadai, E., W. Lehman, and M.J. Rynkiewicz. 2020. Protein-protein docking reveals dynamic interactions of tropomyosin on actin filaments. *Biophys. J.* 119: 77-86.
14. Yamada, Y., K. Namba, and T. Fujii. 2020. Cardiac Muscle thin filament structures reveal calcium regulatory mechanism. *Nature Commun*. 11:153.